Acta Materialia 284 (2025) 120536

Contents lists available at ScienceDirect

Acta Materialia

journal homepage: www.elsevier.com/locate/actamat

Discovery of collective nonjumping motions leading to Johari–Goldstein process of stress relaxation in model ionic glass

Makina Saito [a,b,*], Takeaki Araki [c], Yohei Onodera [b,d], Koji Ohara [e,f], Makoto Seto [b], Yoshitaka Yoda [e], Yusuke Wakabayashi [a]

[a] Department of Physics, Tohoku University, Sendai, Miyagi 980-8578, Japan
[b] Institute for Integrated Radiation and Nuclear Science, Kyoto University, Kumatori, Osaka 590-0494, Japan
[c] Department of Physics, Kyoto University, Kyoto 606-8502, Japan
[d] Center for Basic Research on Materials, National Institute for Materials Science, Tsukuba, Ibaraki 305-0047, Japan
[e] Japan Synchrotron Radiation Research Institute, Sayo, Hyogo 679-5198, Japan
[f] Faculty of Materials for Energy, Shimane University, Matsue, Shimane 690-8504, Japan

ARTICLE INFO

Keywords:
Model ionic glass
Microscopic dynamics experiment
Molecular dynamics simulation
Johari–Goldstein relaxation
Stress relaxation

ABSTRACT

The slow β, or Johari–Goldstein (JG) relaxation process, has been widely observed in glasses and is known to induce the stress relaxation associated with mechanical properties. So far, jumping motions of only a fraction of the particles were believed to contribute to the JG process in glass. However, there is no direct experimental evidence of the atomic-scale images due to the difficulties in microscopic observation. In this study, atomic motions in the quasi-spherical model ionic-glass-former $Ca_{0.4}K_{0.6}(NO_3)_{1.4}$ were microscopically observed with one-angstrom resolution, the highest resolution to date, using X-ray time-domain interferometry. The microscopic experiment directly indicated that most particles underwent angstrom-scale motions in the time scale of the JG relaxation. This result was further supported by molecular dynamics (MD) simulations. A combined study of experiments and MD simulations revealed that most particles contributed to the JG process through unexpected collective nonjumping motions with angstrom-scale displacement, activated by jumping motions of a fraction of particles. The discovery of nonjumping motions by our atomic-scale dynamic observations has considerably advanced our understanding of the puzzling mechanism of the JG process.

1. Introduction

In the liquid–glass transition process, the microscopic structural relaxation time (α-relaxation time) changes largely without an apparent variation in the average structure. In addition to the α process, the angstrom-scale thermally activated process called the slow β process or the Johari–Goldstein (JG) relaxation process has been widely observed in molecular glass-forming systems [1]. It has been shown that the JG process is an essential relaxation process in the glass transition [2], and determines some mechanical properties and fracture mechanics of glasses [3–5]. Furthermore, the JG process plays an essential role in the performance of related materials, such as amorphous phase-change materials [6,7] and superionic conducting glasses [8], as well as in the protein-folding mechanism [9] and the stability of glassy pharmaceuticals and biomaterials [10,11]. Despite the importance of the JG process, there is no consensus regarding its microscopic mechanism [12–14]. Poor knowledge of the JG relaxation prevents the establishment of a universal picture of the glass transition, as numerous theories and models have been proposed to treat the JG process differently or ignore it [2,14–23].

To elucidate the mechanism of JG relaxation, it is crucial to observe JG relaxation in systems composed of spherical particles, for example, colloidal systems, which are the simplest forms of glass formers. However, an apparent signal of the JG relaxation has not been observed in the spherical systems for a long time [18,24]. Recently, the JG process has been discovered in metallic glasses, which are atomistic spherical systems [25], and this discovery has accelerated the study of the JG process [26–29]. In metallic glasses, the JG process causes stress relaxation and determines their mechanical properties and fracture mechanics [26,27]. Some simulation studies have attributed the cooperative jumping motion of a fraction of atomic ions to the origin of the JG process of the stress relaxation in metallic glasses [28,29].

* Correspondiing author at: Department of Physics, Tohoku University, Sendai, Miyagi 980-8578, Japan.
E-mail address: makina.saito.d6@tohoku.ac.jp (M. Saito).

https://doi.org/10.1016/j.actamat.2024.120536
Received 19 April 2024; Received in revised form 11 October 2024; Accepted 3 November 2024
Available online 4 November 2024

However, the complete mechanism of the JG process of stress relaxation, particularly how the jumps of only a fraction of particles are associated with macroscopic stress relaxation, is still not understood because most of the experimental studies of the JG relaxation are based on the macroscopic measurements, which do not provide direct information about the atomic-level dynamics.

To determine whether only a small fraction of the particles was involved in the JG process, we microscopically studied the angstrom-scale dynamics of a model glass-forming system, $Ca_{0.4}K_{0.6}(NO_3)_{1.4}$ (CKN). CKN was chosen because it is a nearly spherical model system consisting of atomic Ca^{2+} and K^+ ions and triangular NO_3^- ions. In addition, because of its very high stability against crystallization, CKN can be studied in higher-temperature supercooled regions compared with metallic glasses [30], complementing active metallic glass research. Angstrom-scale dynamics were directly observed by quasi-elastic scattering experiments with multiline time-domain interferometry (TDI) based on synchrotron radiation [31–33]. Using TDI, the intermediate scattering function (ISF), which is the Fourier transform of the van Hove time–space correlation function, can be observed in the wavenumber q space corresponding to the few angstrom scale. If all particles are involved in the JG process, the ISF decays completely; however, such an observation has not been reported [34–38]. The difficulty in observing ISF decay is due to a decrease in both the scattering intensity and elastic scattering ratio in the high-q region.

In the present study, using the highly efficient multiline TDI method [32], we succeeded in observing the ISF up to $q = 6.3$ Å^{-1}, the highest q value achieved in studies of JG relaxation so far. It was found that the ISF almost fully decays at $q = 6.3$ Å^{-1} in the time scale of the JG process of the stress relaxation, indicating that most particles underwent angstrom-scale motions in the time scale of the JG relaxation. Our expanded observation range, in both length and time scales, presents a new challenge in validating molecular dynamics (MD) results by directly comparing calculations and experiments under the same conditions. MD simulations, which reproduced the experimental results well, revealed the presence of unexpected collective nonjumping motions activated by jumping motions of a fraction of the particles. A combined study of the cutting-edge microscopic experiments and MD simulations revealed that both jumping and nonjumping motions contributed to the partial relaxation of the entire glass structure, resulting in the JG process of macroscopic stress relaxation.

2. Experiment

2.1. Sample preparation

CKN was prepared via a melt-quenching method using $Ca(NO_3)_2$ (99.9 %) and KNO_3 (99.9 %), purchased from Wako Pure Chemical Industries (Japan), following the literature [39]. Anhydrous KNO_3 and $Ca(NO_3)_2$ were heated to 573 K, well above the melting temperature, and maintained for two days. The mixture was then quenched to room temperature at a cooling rate of the order of 10 K s^{-1}. The sample was sealed in a capillary with a diameter of 2 mm (WJM-Glas, Müller GmbH) under an Ar atmosphere for the structural and dynamic experiments.

2.2. X-ray diffraction (XRD) measurements

XRD measurements were performed at 301 K using a high-energy synchrotron radiation X-ray diffraction beamline (BL04B2) at SPring-8, Japan [40]. The energy of the incident X-ray was 61.37 keV. The static structure factor $S(q)$ was obtained from the XRD data after correcting for the effects of polarization and absorption and subtracting the background and contribution of Compton scattering using standard data analysis software [40].

2.3. Microscopic dynamics experiment using multiline TDI

Quasi-elastic gamma-ray scattering experiments using multiline TDI with 14.4-keV Mössbauer gamma rays from ^{57}Fe nuclei were performed at the nuclear resonant scattering beamline (BL09XU) at SPring-8 in Japan [33]. The storage ring was operated in several-bunch timing mode (1/7-filling + 5-bunch mode with bunch intervals of 684.3 ns) with a current of 100 mA. The incident synchrotron radiation was monochromatized to an energy width $\Delta E = 3.5$ meV (full width at half maximum) using a high-resolution monochromator consisting of asymmetric Si (511) and Si (975) channel-cut crystals near the excitation energy. Details of the experiment and analysis can be found in [33]. A double-stacked eight-element Si avalanche photodiode detector was used. The time spectra were measured using a fast multichannel scaler (MCS6; FAST ComTec GmbH, Munich, Germany). The measurement was performed at 320, 330, 340, and 350 K around the glass transition temperature of $T_g = 333$ K at $q = 3.7$ and 6.3 Å^{-1}. A furnace with silicone rubber heaters was used to control the temperature of the sample.

3. Simulation

3.1. Reverse Monte Carlo (RMC) simulation and density functional theory (DFT) calculation

The RMC modeling of the CKN was performed for the experimentally obtained $S(q)$ using the RMC++ code [41]. The initial configuration containing 297 atoms (Ca: 18, K: 27, N: 63, and O: 189) was generated using MD simulations. After RMC modeling, DFT calculations were performed using the projector-augmented wave method implemented in VASP [42]. The generalized gradient approximation functional of Perdew, Burke, and Ernzerhof was used for the exchange-correlation term [43]. A plane-wave cutoff energy of 260 eV was used [44]. The internal atomic positions were optimized until the residual forces were less than <0.1 eV/Å. The RMC and DFT calculations were performed iteratively until the difference in most of the atomic coordination between the RMC and DFT was less than 0.3 Å.

3.2. MD simulation

We performed all-atom MD simulations of CKN using LAMMPS with a time step of 4 fs [45]. The atomic potentials determined in a previous study were used [46]. The numbers of NO_3^-, K^+, and Ca^{2+} ions were N_{NO3} =504, $N_K = 216$, and $N_{Ca} = 144$, respectively. First, the NPT simulation was performed at $T = 700$ K and $p = 1$ atm for 100 ns. A Nosé–Hoover thermostat with a damping parameter of 400 fs was used to control the temperature. The system was then cooled at a rate of −1 K/ns. When the system reached a target temperature T, the cooling was stopped, and the system was annealed for 1 μs. Then, the system was annealed with the NVT simulation at the target temperature for 1 μs prior to product runs. We performed NVT-MD simulation runs starting from different initial states, e.g., 10 runs up to 16 μs at 330 K. To estimate the relaxation times unaffected by the largely out-of-equilibrium states, we averaged the six intermediate values among those in 10 individual product runs, excluding the two largest and smallest ones.

4. Results

Fig. 1a shows the static structure factor $S(q)$ obtained from the XRD experiment as crosses. The $S(q)$ obtained from the final round of the RMC and DFT calculations, shown as a solid line, follows the experimental $S(q)$ well. The modeled glass structure shown in Fig. 1b was used as the static basis for the dynamics experiment and to validate the MD simulation results from a structural viewpoint.

The obtained TDI time spectra are shown in Fig. 2a. The ISFs evaluated at $q = 3.7$ Å^{-1} are shown in Fig. 2b. The decay of the ISF is caused by the displacement of $2\pi/q$ in a simple view. For $q = 3.7$ Å^{-1}, which is

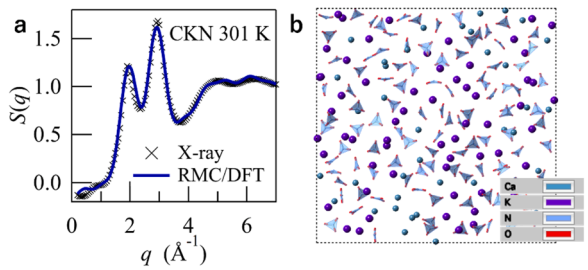

Fig. 1. **a** Experimentally obtained X-ray total static structure factor $S(q)$ obtained at 301 K (crosses). The solid line indicates $S(q)$ obtained using a final round of RMC and DFT calculations, which were performed iteratively. **b** Modeled glass structure of CKN obtained using RMC and DFT calculations.

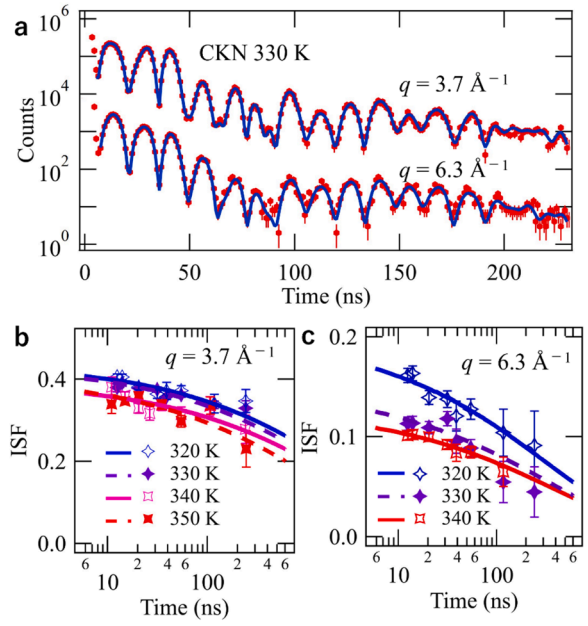

Fig. 2. **a** TDI time spectra obtained at 320 K for $q = 3.7$ and 6.3 Å^{-1} and fitting curves. ISF evaluated from the TDI experiments at **b** $q = 3.7$ Å^{-1} and **c** $q = 6.3$ Å^{-1}, for each temperature. The solid and dashed lines represent the fitting curves.

larger than the peak wavenumber of $S(q)$ ($q \sim 3$ Å^{-1}), the local relaxation motions (with the displacement of few Å) contributing to the JG process have been observed for molecular glass-formers [34–37], some of which have been explained theoretically in Refs. [21–23]. To obtain a detailed JG-relaxation picture, we further aimed to microscopically capture the motion of smaller displacements at the one-angstrom level. In the large-wavenumber region $q > 5$ Å^{-1}, $S(q)$ is nearly unity, as shown in Fig. 1a, indicating that the coherent scattering caused by the mutual atomic correlation is relatively weak there. Thus, the ISF is dominated by the self-term: it follows ISF $\propto \sum_i e^{i\boldsymbol{q}\cdot\{\boldsymbol{r}_i(t)-\boldsymbol{r}_i(0)\}}$, where $\boldsymbol{r}_i(t)$ is the position vector of the particle i at time t. The relaxation of the ISF is known to occur when $|\langle \boldsymbol{r}_i(t) - \boldsymbol{r}_i(0)\rangle| \sim 2\pi/q$ [47]. Hence, we performed the experiment at $q = 6.3$ Å^{-1}, where $2\pi/q \sim 1$ Å, to achieve one-angstrom resolution measurement.

5. Discussion

5.1. Experimental evidence that most particles underwent angstrom-scale motions in the time scale of the JG process

The time spectra were fitted by using a Kohlrausch–Williams–Watts (KWW) function $f\exp\left\{-(t/\tau)^{\beta_{\mathrm{KWW}}}\right\}$ for the relaxation shape of the ISF, where f, τ, and β_{KWW} are the amplitude, relaxation time, and stretching parameter, respectively. The experimentally obtained ISF points and fitting curves are shown in Fig. 2b and 2c, respectively. The average β_{KWW} was obtained to be 0.43±0.08 by averaging all the measured data, and the ISF could be well fitted using the β_{KWW} value. Fig. 3a shows the mean relaxation time $\langle\tau\rangle = \tau\Gamma(1/\beta_{\mathrm{KWW}})/\beta_{\mathrm{KWW}}$ obtained at $q = 3.7$ Å^{-1} (blue circles) and 6.3 Å^{-1} (green triangles) against the temperature T, together with previous relaxation data, such as viscosity, conductivity, dynamic light scattering, and mechanical relaxation spectroscopy (MRS) [48–51]. The statistical standard deviation for each relaxation time is comparable to the size of symbols. Previous studies on molecular glasses observed that the relaxation time at q of the first valley on the high-q side of the $S(q)$ peak agreed well with the JG relaxation time [34,35]. In the present case, the corresponding q is 3.7 Å^{-1} as shown in Fig. 1a. Therefore, $\langle\tau\rangle$ obtained at $q = 3.7$ Å^{-1} (circles) and the JG-relaxation time of MRS (crosses [51]) were simultaneously analyzed using the Arrhenius law. Both data nicely follows the fitting curve as shown in Fig. 3a. Thus, our TDI measurement observed the microscopic relaxation, which is directly related to the macroscopic stress relaxation measured by MRS. This result indicates that the microscopic origin of the stress relaxation is a few angstrom-scale motion. This is consistent with the previous view that the JG-relaxation motion is the local motion [2,14]. Henceforth, the Arrhenius dependence determined here can be treated as the JG-relaxation time τ_{JG}. In addition, $\langle\tau\rangle$ obtained at $q = 6.3$ Å^{-1} falls within this region where the stress relaxation time is distributed (the colored area in Fig. 3a), estimated from the full width at half maximum of the mechanical loss factor obtained previously [51]. Therefore, the relaxations of the ISF observed at $q = 3.7$ and 6.3 Å^{-1} reflect that the angstrom-scale atomic motions contribute to the JG process in the stress relaxation.

To determine whether only a small fraction of particles is involved in the JG process, it is crucial to observe whether only a part of the ISF is relaxed by the JG process. Fig. 3b shows the ISFs normalized by τ (horizontal axis) and f (vertical axis) for $q = 3.7$ Å^{-1} (blue squares) and 6.3 Å^{-1} (green triangles) at all the temperatures. The relaxation form can be visualized well using a normalization plot. The figures show that all the points collapse to the single KWW function with the experimentally obtained $\beta_{\mathrm{KWW}} = 0.43$ (dotted line) at both $q = 3.7$ and 6.3 Å^{-1}. At $q = 3.7$ Å^{-1}, the final part of the relaxation of the ISF is not in the observation time window, as shown in Figs. 2b and 3b (right). Previous TDI studies have suffered from the same problem [34–37]. In contrast, Fig. 2c shows that the ISF obtained at $q = 6.3$ Å^{-1} decays at least to 0.05, close to 0. The normalization plot in Fig. 3b (left) shows a nearly complete decay at $q = 6.3$ Å^{-1}. In general, the larger the q (the smaller the length scale in which the specific relaxation mode is studied), the shorter the time scale of the relaxation motions with the displacement of the selected length scale $\sim 2\pi/q$ in the simplest case. Consequently, the relaxation time at $q = 6.3$ Å^{-1} was within the experimental time window. Fig. 3b (left) shows that the normalized ISF decays to at least 0.25, indicating that at least 75 % of the particles underwent the corresponding angstrom-scale motion on the time scale of the JG process. If the previous explanation that only a portion of the jumping particles contributed to JG relaxation and other particles are stational is applied [28,29], at least 75 % of the jump particles must be present in the system. This prevents the system from remaining in a glassy state, contrary to the fact that glassy CKN was studied. Therefore, the experiment indicated that nonjumping particles must move also in the time scale of the JG relaxation through angstrom-scale motions. This result is further supported by the following MD simulations.

5.2. Experimental validation of the MD simulation results

To experimentally validate the MD simulation results, we first compared the static structures obtained using the RMC/DFT calculations based on the X-ray static structure factor and typical MD simulation. Fig. 4a shows the pair-distribution function $g_{\alpha\beta}(r)$ for each atomic pair

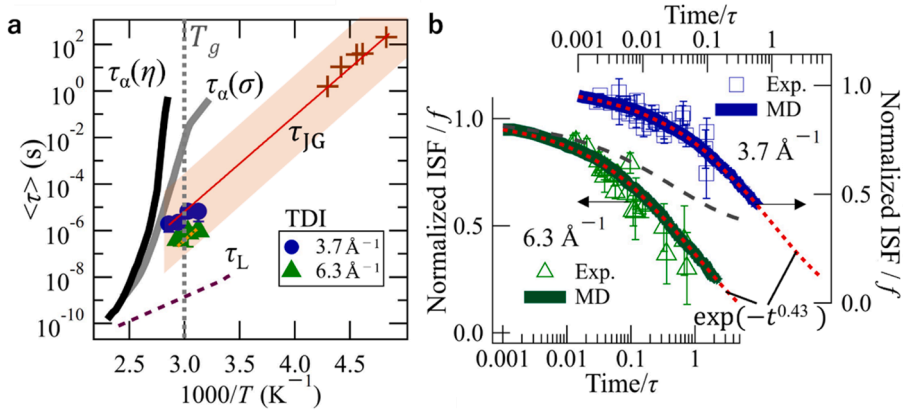

Fig. 3. **a** Mean relaxation time vs. 1000/T obtained using TDI at $q = 3.7$ Å^{-1} (blue circles) and 6.3 Å^{-1} (green triangles). The bold curves denote the α-relaxation times associated with viscosity ($\tau_\alpha(\eta)$, black) [48] and conductivity ($\tau_\alpha(\sigma)$, gray) [49]. The dashed line labeled τ_L represents the time scale of the libration motion [50]. The dark brown crosses are the JG relaxation times τ_{JG} obtained using MRS [51]. The red straight line represents the fitting curve obtained using the Arrhenius law for the JG relaxation time obtained by MRS and $\langle\tau\rangle$ obtained at $q = 3.7$ Å^{-1}. The colored area shows the region where the JG relaxation time of the stress is distributed [51]. **b** Experimental ISFs normalized with τ and f are plotted for 3.7 Å^{-1} (right panel, blue squares), and 6.3 Å^{-1} (left panel, green triangles) at all temperatures near T_g. The KWW function with $\beta_{KWW} = 0.43$ is also plotted (red dotted curve). The solid thick lines are the normalized ISFs obtained using the MD simulation at the corresponding q. The black dashed line in the left panel is the relaxation shape evaluated for the case where only the J particles moved.

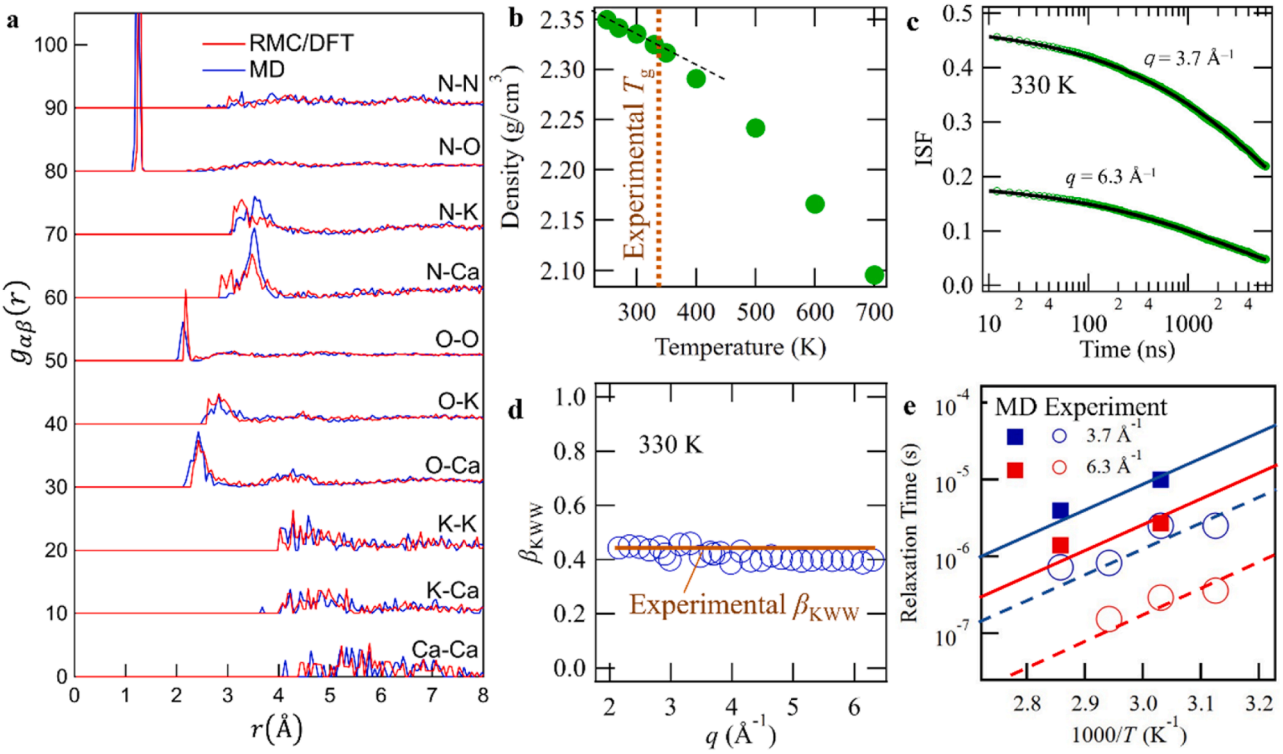

Fig. 4. **a** Partial pair-distribution function $g_{\alpha\beta}(r)$ of CKN. The blue and red lines are $g_{\alpha\beta}(r)$ obtained from the glass structure of MD calculations and RMC/DFT calculations based on the X-ray static structure factor, respectively. **b** Temperature dependence of the density obtained using the MD simulation. The dotted line indicates the glass transition temperature T_g. The dashed line is the guide for eyes. **c** ISFs obtained using MD simulation at 330 K for $q = 3.7$ and 6.3 Å^{-1} (circles). Solid curves are fitting curves. **d** β_{KWW} obtained using MD simulation as a function of q. The horizontal line shows the experimentally obtained β_{KWW} value. **e** Temperature dependence of the relaxation time obtained using MD simulations at $q = 3.7$ Å^{-1} (blue squares) and 6.3 Å^{-1} (red squares). The experimental relaxation times are also shown as blue and red circles for the data obtained at the corresponding q. The lines are the Arrhenius curves with the activation energy of the JG process.

obtained using the MD simulation and the RMC/DFT calculation for the X-ray diffraction data, where α and β indicate the atomic species, and r is the distance. Both $g_{\alpha\beta}(r)$ results agree with each other. In addition, T_g was evaluated from the temperature at which the temperature dependence of the density began to deviate from the solid-like linear temperature dependence (dashed line) upon heating. The evaluated glass transition temperature agrees well with the experimental T_g of 333 K, as indicated by the dotted line in Fig. 4b.

Subsequently, we compared the dynamic results obtained from the TDI and MD simulations. The ISFs were calculated from the MD simu-

lation results by considering the X-ray scattering amplitude of each atom. The ISFs obtained at 330 K and $q = 3.7$ and 6.3 Å^{-1} are shown in Fig. 4c. The relaxation time of the ISF was estimated by fitting with the KWW function with a free β_{KWW} parameter as shown in the fitting results in Fig. 4c. Fig. 4d shows the q dependence of β_{KWW} obtained using MD simulation. We observed that β_{KWW} hardly depends on q and temperature, and is consistent with the experimental value of 0.43 (horizontal line). To visualize the consistency of the relaxation form, the MD-simulated ISFs normalized with τ and f at 330 K for $q = 3.7$ and 6.3 Å^{-1} are plotted as thick lines in Fig. 3b. The relaxation form of the ISF closely follows the KWW master curve of the experimental ISF. This result also indicates the same relaxation form for the experimental and simulated ISFs. Fig. 4e shows the temperature dependence of the relaxation time obtained at $q = 3.7$ and 6.3 Å^{-1}. These data are consistent with the Arrhenius behavior, with the experimental activation energy shown as lines [51]. Given that no adjustment parameters were used, the relaxation times obtained from the MD simulations were in sufficient agreement within the scope of the following discussion on the atomic origin of the JG process.

5.3. *Dynamic and structural heterogeneity observed in the time scale of the JG relaxation using MD simulations*

Fig. 5a shows the trajectories of the center of the particles obtained using the typical MD simulation run within a duration of 12 μs, which is longer than the time scale of $\tau_{JG} \sim 6$ μs at 330 K in the glass state. We averaged the atomic positions every 4 ns to eliminate the vibrational motion in the cages and the fast rotational motion of the NO_3 ions, which occur at much faster time scales [49]. This makes it easier to observe the shift in the center of the particles: N, K, and Ca atoms. The straight lines with the length of the interparticle distance (~3–4 Å) represent the interparticle-scale jumping motions, which were observed to occur cooperatively, e.g., in loop-like and string-like ways. Such jumping motions have been observed in various systems, including metallic glasses [28,52–54]. We defined a motion whose displacement over a duration of 4 ns was larger than 2.5 Å as a jumping motion. Fig. 5b shows a magnified image of a part of the trajectory map with the atoms in the initial position. For example, both jumping and nonjumping types of K atoms were present on the timescale of the JG process, as indicated by the arrows. Fig. 5c shows the time-dependent atomic displacement of a particle experiencing jumps (red) and no jumps (black). We observed that almost half of the particles experienced a jump, whereas the others did not experience a jump in CKN on the timescale. These particles are hereafter referred to as J and NJ particles only for convenience in discussing the properties of particles in different states of motion (experienced jumps or not), keeping in mind that the classification holds only on the timescale of the JG process. Fig. 5a also shows the density field of the J particles; the darker the color, the higher the density of the J particles. The figure shows that the J particles aggregate at the nanometric scale (i.e., dynamic heterogeneity is present). Nanometer-scale clusters of J particles are also observed in metallic glasses [55].

To investigate the presence of static heterogeneity behind the dynamic heterogeneity, we calculated the partial pair-distribution functions $g(r)$ for the J–J and NJ–NJ particle pairs. The results obtained at 330 K are shown in Fig. 5d. The $g(r)$ peaks of the J–J particle pairs were lower than those of the NJ–NJ particle pairs, indicating that the coordination number of the J particles was smaller than that of the NJ particles. Therefore, in the J-particle-rich region, the J particles were relatively loosely packed. This result explains the structural reason why the J particles jump frequently. Thus, we observed static heterogeneity behind dynamic heterogeneity in CKN. A similar result has been observed for metallic glass, where excess free volume leads to the activation of the atomic motions such as the JG relaxation [56] through the formation of the shear transformation zone (STZ) [57–59], boson peak, and fast β relaxation [60–62].

Fig. 5e shows the average mean square displacement (MSD) of the J (solid line) and NJ (dashed line) types of N, K, and Ca atoms as functions of time. The mobility depends on the particle species, e.g. Ca is the

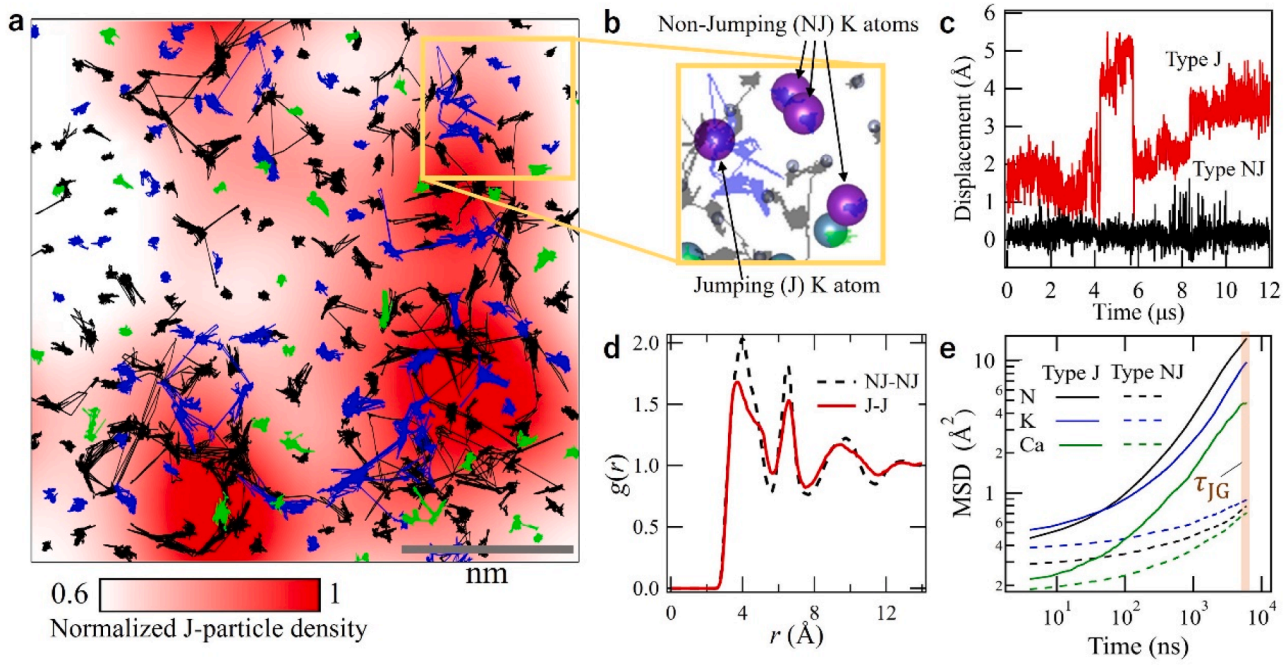

Fig. 5. **a** Displacement maps obtained using MD simulation over the duration of 12 μs at 330 K. The black, blue, and green trajectories are for N, K, and Ca atoms, respectively. The oxygen atoms are omitted to visualize the translational motions. The density field of the J particles is also shown. **b** Enlarged displacement maps with atoms in initial positions. The jumping and nonjumping K atoms are indicated. **c** Time dependence of the atomic displacement of a typical J particle, which experiences the interparticle-scale jump, and a typical NJ particle, which does not experience the jump. **d** Pair-distribution functions evaluated for the J–J particle pairs and NJ–NJ particle pairs. **e** Time-dependent MSD for J (solid line) and NJ (dashed line) types for N, K, and Ca atoms as a function of time. The JG relaxation time τ_{JG} is also shown as the vertical line.

slowest species, as previously reported for the α process [63]. As expected, the J particles were faster than the NJ particles due to the jumping motions. Because the difference between the J and NJ species is larger than that between the atomic species, atomic species are not considered hereafter.

5.4. MD simulation support for experimental observation that most NJ particles underwent angstrom-scale motions in the time scale of JG relaxation

Experiments have shown that the most NJ particles underwent angstrom-scale motion in the time scale of the JG relaxation. In this section, the experimental conclusion is further supported by the MD simulations. We first investigated whether the NJ particles, which accounted for half of the total particles, were stationary in the CKN, as proposed for metallic glasses. Accordingly, the ISF was evaluated by assuming that the NJ particles observed in the MD simulation were treated as stationary and only the J particles moved with the simulated relaxation time. The evaluated ISF is indicated by the black dashed line in Fig. 3b (left). The simulated ISF deviates from the experimental ISF, and is inconsistent with the experimental observation that the ISF decays almost completely (by at least 75 %). Thus, MD simulation also supports the experimental conclusion.

5.5. Evidence that most NJ particles contribute to the JG process as found in MD simulation

To directly investigate whether the NJ-particle motion significantly contributed to the JG process of stress relaxation, the autocorrelation function of the shear stress $G_{NJ}(t)$ was calculated using the Green-Kubo formula in the MD simulations for each NJ particle. Fig. 6a shows the histogram of the $G_{NJ}(t)$ value of all NJ particles at $t = 0$ s, 4 ns, and 6 μs ($\sim \tau_{JG}$). The figure shows that stress relaxation occurs in most NJ particles in the time scale of the JG process, i.e., 6 μs.

Next, we investigated the correlation between the motions of the J and NJ particles to understand the mechanism by which NJ particles contributed to the JG process. Fig. 6b and 6c show the MSD and the non-Gaussian parameter (α_2, indicating the degree of deviation from Gaussian dynamics) obtained for the J and NJ particles, respectively. The α_2 of the J particles shows a clear peak. This is a well-known behavior associated with cage rearrangement: α_2 reaches a peak at the time scale of cage rearrangement τ^J_{cage} by inter-particle scale jump motions [64] associated with the JG process in the present case [28]. Owing to the onset of the jumping motions, the MSD for the J particles increase substantially just after τ^J_{cage}, as can be seen in Fig. 6b. In contrast, the α_2 of the NJ particles does not show an apparent peak, indicating that the dynamics of the NJ particles do not include jumping motions, which is consistent with the definition of NJ particles. This reflects the fact that the NJ particles are not directly associated with the cage rearrangement. Hence, it can be expected that after τ^J_{cage}, the J particles' dynamic behavior, such the time dependence of MSD, becomes different from that of the NJ particles.

However, we found a clear relationship between the MSDs of these particles, even after τ^J_{cage}. Fig. 6d shows the MSDs of the J and NJ particles, MSD_J and MSD_{NJ}, plotted against each other at each time before and after τ^J_{cage}. A linear relationship in the log–log plot (in other words, $MSD_{NJ} \propto MSD_J{}^x$ with $x \sim 0.26$) is visible across the MSD values at τ^J_{cage}, which is marked by the large cross symbol. This linearity across the MSD values at τ^J_{cage} is surprising, because the dynamics of the J particles are associated with the cage rearrangement jumping motion, whereas those of the NJ particles are not directly associated with it.

The observed unexpected relationship of the MSDs indicates that the jumping motion accelerates the motion of the NJ particles after τ^J_{cage}. One of the simplest mechanisms for this unexpected relationship is that, after a J particle jumps, the NJ particles adjacent to the J particle move slightly toward the vacancy created by the jump [65]. Subsequent jumps to the vacancy result in local structures slightly different from the initial ones because of the local motion of the NJ particles. The repetition of these processes gradually causes partial relaxation of the entire glass structure. If there is no NJ particle motion, the J particles merely jump back and forth, resulting in no change in the stress correlation of the surrounding matrix. Hence, we conclude that the motion of the NJ particles plays a significant role in stress relaxation.

At the end of this section, we validate the angstrom-level resolution of our measurements based on simulation. The relaxation time of the ISF at $q = 6.3$ Å^{-1}, shown in Fig. 4e, is 2.7 μs. The average amplitude of the NJ-particle motion at the relaxation time was estimated as ~ 0.7 Å from the square root of the MSD value of 2.7 μs, as shown in Fig. 5e. The displacement was of the order of angstroms. Thus, we validated that the angstrom-level displacement of the NJ particles could be detected by

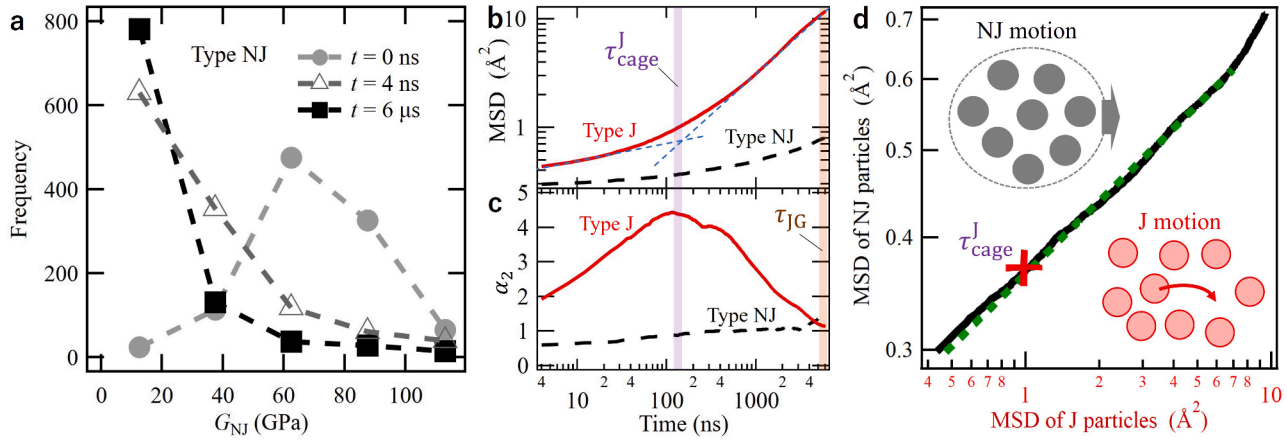

Fig. 6. **a.** Histogram of the $G_{NJ}(t)$ value of NJ particles at $t = 0$ s, 4 ns, and 6 μs ($\sim \tau_{JG}$). **b.** MSD and **c.** non-Gaussian parameter α_2 as a function of time obtained by MD simulations at 330 K in glass state. The vertical purple and orange lines indicate the cage rearrangement time τ^J_{cage} of the J particles and macroscopic stress (JG) relaxation time τ_{JG}, respectively. The thin dashed lines are eye guides. **d.** Correlation between the MSDs of the J and NJ particles: a log–log plot of the MSDs of the J and NJ particles plotted against each other at each time point. Schematics of the dynamics of the J and NJ particles are presented. Cross-point MSD values at the cage rearrangement time τ^J_{cage}. The dashed line represents a power-law fit.

obtaining the ISF at $q = 6.3$ Å^{-1}.

5.6. Collectivity of nonjumping motions

To investigate the real space picture of NJ-particle motion, we show the displacement vectors of the particles over 6 μs, the time scale of τ_{JG}, at 330 K in Fig. 7a. The empty and filled arrows indicate the displacement vectors of the J and NJ particles, respectively. The initial and final atomic positions averaged over 4 ns were used to calculate the displacement vectors in the same manner as in the calculated trajectory map. In addition, the displacement vector length of the NJ particles was increased by a factor of five for visibility. Collective motions in the same direction were observed, as shown in the regions highlighted by blue ellipses. We found the collective motion occurs selectively in the NJ-particle-rich region (less-colored region of the J-particle density field) visualizing the dynamic collectivity of the NJ particles.

To quantify the degree of collectivity, the spatial correlation function of the particle displacement direction

$$H(r,t) = \frac{V}{4\pi r^2 N_p^2 g(r)} \sum_{i\neq j} \left\langle \Delta\hat{\boldsymbol{r}}_i(t)\cdot\Delta\hat{\boldsymbol{r}}_j(t)\delta\left(r - \left|\boldsymbol{r}_i(0) - \boldsymbol{r}_j(0)\right|\right)\right\rangle$$

was calculated by analyzing the trajectory, where $\Delta\hat{\boldsymbol{r}}_i(t)$ is the unit vector along the displacement $\Delta\boldsymbol{r}_i(t) = \boldsymbol{r}_i(t) - \boldsymbol{r}_i(0)$ obtained for a particle i at time t, $\boldsymbol{r}_i(t)$ is the position at t, $g(r)$ is the pair distribution function, and N_p is the total number of particles. When the ions move collectively with the neighboring ions, $H(r,t)$ increases toward unity, and the decay length of $H(r,t)$ in the r-dependent plot provides the correlation size of the collective motions at the time scale of t. Fig. 7b shows the r-dependent plot of $H(r,\tau_{JG})$ for the J and NJ particles. The figure shows that the NJ particles collectively move considerably more than the J particles on the timescale. This quantitatively demonstrates the collective nature of the nonjumping motions, as observed in Fig. 7a. The average volume occupied by the collectively moving particles, $\langle V_c\rangle$, was evaluated at τ_{JG} as $\langle V_c\rangle = \int dr 4\pi r^2 H(r,\tau_{JG})$. $\langle V_c\rangle$ is approximately 500 Å^3 = (7.9 Å)^3, involving several tens of ions. This average size of sub nanometer is equivalent to that of the ellipsoidal regions shown in Fig. 7a. Therefore, the collective relaxation motions shown in the figure are not rare events but occur frequently. The collective relaxation nature of the NJ particles can be assumed as the mechanism by which most particles are involved in JG relaxation.

So far, the microscopic origin of the JG process of stress relaxation has been attributed to the jumping motions in the J-particle-rich region, which is known as STZ, based on a good agreement between the potential energy barrier of the STZ and the activation energy of the JG relaxation [59]. This agreement was explained by the fluctuation-dissipation theorem, which states that, in the weak stress limit, stress relaxation originates from structural relaxation (the jumping motions in the present case) which is intrinsic in the absence of external stress. However, if the jumping motions occur only in a part of regions and most of the particles in another region are stationary, the macroscopic stress is not effectively relaxed. Our results showed for the first time that the collective nonjumping motion of the surrounding particles is also activated by the jumping motions, as shown schematically in Fig. 7c. It was found that repetitions of both types of motions induced the partial relaxation of the entire glass structure resulting in the JG process of macroscopic stress relaxation. Our direct observation of atomic motions considerably advanced our insight into the JG process, with the support of MD simulations.

6. Conclusion

We succeeded in directly observing the atomic motions responsible for JG process of stress relaxation in the quasi-spherical model ionic-glass-forming system CKN with one-angstrom resolution. We observed that most particles underwent angstrom-scale motions in the time scale of the JG process in CKN. MD simulations, which are consistent with the experiments in many aspects, revealed that both well-known jumping motions and collective nonjumping motions induced by the jumping motions contributed to the JG process. This finding clarifies the link between the JG process of the macroscopic stress relaxation under external stress and microscopic relaxations in the absence of external stress. We also found that CKN shares similar characteristics with metallic glasses, such as the presence of jumping particles, the cooperativity of jumping motions, nanometer-scale dynamic heterogeneity, and the relationship between static and dynamic heterogeneities. Therefore, it is extremely important to investigate the nonjumping

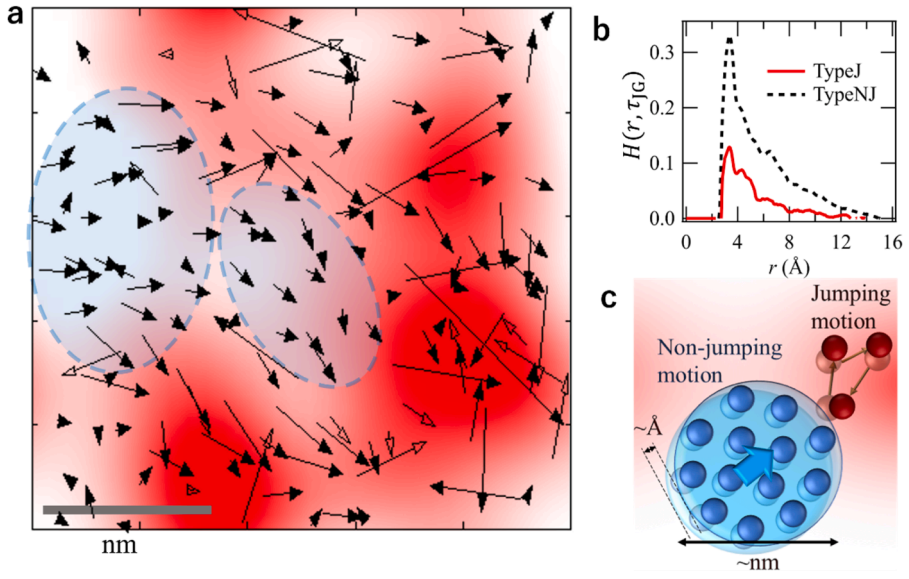

Fig. 7. **a** Displacement map obtained using MD simulations over the durations of 6 μs near τ_{JG} with a density field of J particles at 330 K. The filled and empty arrows represent nonjumping and jumping motions, respectively. The displacement vector length of the NJ particles was increased by a factor of five for visibility. The oxygen atoms are ignored to visualize the translational motions. The regions where the particles collectively move in the same direction are highlighted by blue ellipses. **b** Spatial correlation function of the displacement direction $H(r,\tau_{JG})$ obtained using MD simulation at 330 K for types J and NJ, respectively. **c** Schematic of the jumping and nonjumping motions in the duration of τ_{JG}.

motion of metallic glasses in the future for a more universal understanding of the JG relaxation.

CRediT authorship contribution statement

Makina Saito: Writing – original draft, Validation, Resources, Project administration, Methodology, Investigation, Funding acquisition, Formal analysis, Data curation, Conceptualization. **Takeaki Araki:** Writing – review & editing, Visualization, Validation, Methodology, Investigation, Formal analysis, Data curation. **Yohei Onodera:** Writing – review & editing, Visualization, Investigation, Formal analysis, Data curation. **Koji Ohara:** Writing – review & editing, Visualization, Investigation, Formal analysis, Data curation. **Makoto Seto:** Writing – review & editing, Supervision, Resources. **Yoshitaka Yoda:** Investigation. **Yusuke Wakabayashi:** Writing – review & editing.

Declaration of competing interest

The authors declare that they have no known competing financial interests or personal relationships that could have appeared to influence the work reported in this paper.

Acknowledgments

The authors are grateful to T. Yanagishima (Kyoto University), U. K. Nandi (Kyoto University), A. Ikeda (Tokyo University), and H. Tanaka (Tokyo University) for helpful discussions and critical reading of this manuscript. This study was approved by the Japan Synchrotron Radiation Research Institute (2016A1084, 2016A1461, 2019B2100, 2020A0694, 2020A1329). This study was supported by JSPS KAKENHI [Grant Numbers 21K03486 and 24K00592], the Iwatani Naoji Foundation, and JST CREST [Grant Number JPMJCR2095], Japan. Some computations in this study were performed using the facilities at the Supercomputer Center, Institute for Solid-State Physics, University of Tokyo, Japan.

References

[1] G.P. Johari, M. Goldstein, Viscous liquids and the glass transition. II. Secondary relaxations in glasses of rigid molecules, J. Chem. Phys. 53 (1970) 2327–2388.
[2] K.L. Ngai, Relaxation and Diffusion in Complex Systems, Springer, Berlin, 2011.
[3] R.F. Boyer, Dependence of mechanical properties on molecular motion in polymers, Polym. Eng. Sci. 8 (1968) 161–185.
[4] C. Xiao, J.Y. Jho, A.F. Yee, Correlation between the shear yielding behavior and secondary relaxations of bisphenol A polycarbonate and related copolymers, Macromolecules 27 (1994) 2761–2768.
[5] M. Böhning, U. Niebergall, A. Adam, W. Stark, Influence of biodiesel sorption on temperature-dependent impact properties of polyethylene, Polym. Test. 40 (2014) 133–142.
[6] S.X. Peng, Y. Cheng, J. Pries, S. Wei, H.B. Yu, M. Wuttig, Uncovering β-relaxations in amorphous phase-change materials, Sci. Adv. 6 (2020) eaay6726.
[7] Y. Cheng, Q. Yang, J. Wang, T. Dimitriadis, M. Schumacher, H. Zhang, M.J. Müller, N. Amini, F. Yang, A. Schoekel, J. Pries, R. Mazzarello, M. Wuttig, H.B. Yu, S. Wei, Highly tunable β-relaxation enables the tailoring of crystallization in phase-change materials, Nat. Commun. 13 (2022) 7352.
[8] J. Habasaki, C. León, K.L. Ngai, Dynamics of Glassy, Crystalline and Liquid Ionic Conductors: Experiments, Theories, Simulations, Springer, Switzerland, 2017.
[9] P.W. Fenimore, H. Frauenfelder, B.H. McMahon, R.D. Young, Bulk-solvent and hydration-shell fluctuations, similar to α- and β-fluctuations in glasses, control protein motions and functions, Proc. Natl. Acad. Sci. USA 101 (2004) 14408–14413.
[10] M.T. Cicerone, J.F. Douglas, β-Relaxation governs protein stability in sugar-glass matrices, Soft Matter 8 (2012) 2983–2991.
[11] S. Bhattacharya, R. Suryanarayanan, Local mobility in amorphous pharmaceuticals–characterization and implications on stability, J. Pharm. Sci. 98 (2009) 2935–2953.
[12] K. Shiraishi, H. Mizuno, A. Ikeda, Johari–Goldstein relaxation in glassy dynamics originates from two-scale energy landscape, Proc. Natl. Acad. Sci. USA 120 (2023) e2215153120.
[13] Y. Chen, Z. Ye, K. Wang, J. Huang, H. Tong, Y. Jin, K. Chen, H. Tanaka, P. Tan, Visualizing slow internal relaxations in a two-dimensional glassy system, Nat. Phys. 19 (2023) 969.
[14] K.L. Ngai, Universal properties of relaxation and diffusion in complex materials: originating from fundamental physics with rich applications, Prog. Mater. Sci. 139 (2023) 101130.
[15] S.H. Chong, Connections of activated hopping processes with the breakdown of the Stokes-Einstein relation and with aspects of dynamical heterogeneities, Phys. Rev. E 78 (2008) 041501.
[16] H. Tanaka, Origin of the excess wing and slow β relaxation of glass formers: a unified picture of local orientational fluctuations, Phys. Rev. E 69 (2004) 021502.
[17] J.D. Stevenson, P.G. Wolynes, A universal origin for secondary relaxations in supercooled liquids and structural glasses, Nat. Phys. 6 (2010) 62–69.
[18] B. Guiselin, C. Scalliet, L. Berthier, Microscopic origin of excess wings in relaxation spectra of supercooled liquids, Nat. Phys. 18 (2022) 468–474.
[19] P. Charbonneau, Y. Jin, G. Parisi, C. Rainone, B. Seoane, F. Zamponi, Numerical detection of the Gardner transition in a mean-field glass former, Phys. Rev. E 92 (2015) 012316.
[20] K. Geirhos, P. Lunkenheimer, A. Loidl, Johari-Goldstein relaxation far below T_g: experimental evidence for the Gardner transition in structural glasses? Phys. Rev. Lett. 120 (2018) 085705.
[21] K.L. Ngai, S. Capaccioli, M. Paluch, L. Wang, Clarifying the nature of the Johari-Goldstein β-relaxation and emphasising its fundamental importance, Philos. Mag. 100 (2020) 2596–2613.
[22] K.L. Ngai, Microscopic understanding of the Johari-Goldstein β relaxation gained from nuclear γ-resonance time-domain-interferometry experiments, Phys. Rev. E 104 (2021) 015103.
[23] K.L. Ngai, S. Capaccioli, P. Lunkenheimer, A. Loidl, Arriving at the most plausible interpretation of the dielectric spectra of glycerol with help from quasielastic γ-ray scattering time-domain interferometry, Phys. Rev. E 105 (2022) 054609.
[24] G.L. Hunter, E.R. Weeks, The physics of the colloidal glass transition, Rep. Prog. Phys. 75 (2012) 066501.
[25] Z. Wang, H.B. Yu, P. Wen, H.Y. Bai, W.H. Wang, Pronounced slow β-relaxation in La-based bulk metallic glasses, J. Phys. Condens. Matter 23 (2011) 142202.
[26] H.B. Yu, X. Shen, Z. Wang, L. Gu, W.H. Wang, H.Y. Bai, Tensile plasticity in metallic glasses with pronounced β relaxations, Phys. Rev. Lett. 108 (2012) 015504.
[27] W.H. Wang, Dynamic relaxations and relaxation-property relationships in metallic glasses, Prog. Mater. 106 (2019) 100561.
[28] H.B. Yu, R. Richert, K. Samwer, Structural rearrangements governing Johari-Goldstein relaxations in metallic glasses, Sci. Adv. 3 (2017) e1701577.
[29] Y. Sun, S.X. Peng, Q. Yang, F. Zhang, M.H. Yang, C.Z. Wang, K.M. Ho, H.B. Yu, Predicting complex relaxation processes in metallic glass, Phys. Rev. Lett. 123 (2019) 105701.
[30] P. Lu, Y. Zhai, P. Falus, V.G. Sakai, M. Hartl, M. Kofu, K. Nakajima, A. Faraone, Y Z, Q-dependent collective relaxation dynamics of glass-forming liquid $Ca_{0.4}K_{0.6}(NO_3)_{1.4}$ investigated by wide-angle neutron spin-echo, Nat. Commun. 13 (2022) 2092.
[31] A.Q.R. Baron, H. Franz, A. Meyer, R. Rüffer, I. Chumakov, E. Burkel, W. Petry, Quasielastic scattering of synchrotron radiation by time domain interferometry, Phys. Rev. Lett. 79 (1997) 2823–2826.
[32] M. Saito, M. Seto, S. Kitao, Y. Kobayashi, M. Kurokuzu, Y. Yoda, Time-domain interferometry experiments using multi-line nuclear absorbers, Hyperfine Interact. 206 (2012) 87–90.
[33] M. Saito, R. Masuda, Y. Yoda, M. Seto, Synchrotron radiation-based quasi-elastic scattering using time-domain interferometry with multi-line gamma rays, Sci. Rep. 7 (2017) 12558.
[34] M. Saito, S. Kitao, Y. Kobayashi, M. Kurokuzu, Y. Yoda, M. Seto, Slow processes in supercooled o-terphenyl: relaxation and decoupling, Phys. Rev. Lett. 109 (2012) 115705.
[35] T. Kanaya, R. Inoue, M. Saito, M. Seto, Y. Yoda, Relaxation transition in glass-forming polybutadiene as revealed by nuclear resonance X-ray scattering, J. Chem. Phys. 140 (2014) 144906.
[36] M. Saito, M. Kurokuzu, Y. Yoda, M. Seto, Microscopic observation of hidden Johari-Goldstein-β process in glycerol, Phys. Rev. E 105 (2022) L012605.
[37] F. Caporaletti, S. Capaccioli, S. Valenti, M. Mikolasek, A.I. Chumakov, G. Monaco, Experimental evidence of mosaic structure in strongly supercooled molecular liquids, Nat. Commun. 12 (2021) 1867.
[38] R. Mashita, M. Saito, Y. Yoda, N. Nagasawa, Y. Bito, T. Kikuchi, H. Kishimoto, M. Seto, T. Kanaya, Microscopic observation of the anisotropy of the Johari-Goldstein-β process in cross-linked polybutadiene on stretching by time-domain interferometry, ACS Macro Lett. 13 (2024) 847–852.
[39] C. Tengroth, J. Swenson, A. Isopo, L. Börjesson, Structure of $Ca_{0.4}K_{0.6}(NO_3)_{1.4}$ from the glass to the liquid state, Phys. Rev. B 64 (2001) 224207.
[40] S. Kohara, M. Itou, K. Suzuya, Y. Inamura, Y. Sakurai, Y. Ohishi, M. Takata, Structural studies of disordered materials using high-energy x-ray diffraction from ambient to extreme conditions, J. Phys. Condens. Matter 19 (2007) 506101.
[41] O. Gereben, P. Jóvári, L. Temleitner, L. Pusztai, A new version of the RMC++ Reverse Monte Carlo program, aimed at investigating the structure of covalent glasses, J. Optoelectron. Adv. Mater. 9 (2007) 3021–3027.
[42] P.E. Blöchl, Projector augmented-wave method, Phys. Rev. B 50 (1994) 17953–17979.
[43] J.P. Perdew, K. Burke, M. Ernzerhof, Generalized gradient approximation made simple, Phys. Rev. Lett. 77 (1996) 3865–3868.
[44] K. Ohara, A. Mitsui, M. Mori, Y. Onodera, S. Shiotani, Y. Koyama, Y. Orikasa, M. Murakami, K. Shimoda, K. Mori, T. Fukunaga, H. Arai, Y. Uchimoto, Z. Ogumi, Structural and electronic features of binary Li_2S-P_2S_5 glasses, Sci. Rep. 6 (2016) 21302.
[45] LAMMPS molecular dynamics package, (2024) lammps.sandia.gov.

[46] G.F. Signorini, J.L. Barrat, M.L. Klein, Structural relaxation and dynamical correlations in a molten state near the liquid-glass transition: a molecular dynamics study, J. Chem. Phys. 92 (1990) 1294–1303.
[47] M.T.F. Telling, A Practical Guide to Quasi-Elastic Neutron Scattering, Royal Society of Chemistry, London, 2020.
[48] E.A. Pavlatou, A.K. Rizos, G.N. Papatheodorou, G. Fytas, Dynamic light scattering study of ionic KNO_3–$Ca(NO_3)_2$ mixtures, J. Chem. Phys. 94 (1991) 224–232.
[49] A. Pimenov, P. Lunkenheimer, H. Rall, R. Kohlhaas, A. Loidl, R. Böhmer, Ion transport in the fragile glass former $3KNO_3$-$2Ca(NO_3)_2$, Phys. Rev. E 54 (1996) 676–684.
[50] P. Jacobsson, L. Börjesson, A.K. Hassan, L.M. Torell, Reorientational motion of the NO_3 ion through the liquid-glass transition in $Ca_{0.4}K_{0.6}(NO_3)_{l.4}$ and $Ca(NO_3)_2 + 8H_2O$, J. Non-Cryst. Solids 172–174 (1994) 161–164.
[51] C. Mai, S. Etienne, J. Perez, G.P. Johari, Mechanical relaxation in an ionic glass, Philos. Mag. B 50 (1985) 657–663.
[52] C. Donati, J.F. Douglas, W. Kob, S.J. Plimpton, P.H. Poole, S.C. Glotzer, Stringlike cooperative motion in a supercooled liquid, Phys. Rev. Lett. 80 (1998) 2338–2341.
[53] W. Kob, C. Donati, S.J. Plimpton, P.H. Poole, S.C. Glotzer, Dynamical heterogeneities in a supercooled Lennard-Jones liquid, Phys. Rev. Lett. 79 (1997) 2827–2830.
[54] P.Z. Hanakata, J.F. Douglas, F.W. Starr, Interfacial mobility scale determines the scale of collective motion and relaxation rate in polymer films, Nat. Commun. 5 (2014) 4163.
[55] Z. Wang, B.A. Sun, H.Y. Bai, W.H. Wang, Evolution of hidden localized flow during glass-to-liquid transition in metallic glass, Nat. Commun. 5 (2014) 5823.
[56] X.D. Wang, B. Ruta, L.H. Xiong, D.W. Zhang, Y. Chushkin, H.W. Sheng, H.B. Lou, Q.P. Cao, J.Z. Jiang, Free-volume dependent atomic dynamics in beta relaxation pronounced La-based metallic glasses, Acta Mater. 99 (2015) 290–296.
[57] A.S. Argon, Plastic deformation in metallic glasses, Acta Metall. 27 (1979) 47–58.
[58] M.L. Falk, J.S. Langer, Dynamics of viscoplastic deformation in amorphous solid, Phys. Rev. E 57 (1998) 7192–7205.
[59] H.B. Yu, W.H. Wang, H.Y. Bai, Y. Wu, M.W. Chen, Relating activation of shear transformation zones to β relaxations in metallic glasses, Phys. Rev. B 81 (2010) 220201R.
[60] P. Palomino Rico, D.G. Papageorgiou, A.L. Greer, G.A. Evangelakis, The atomistic mechanism of fast relaxation processes in $Cu_{65}Zr_{35}$ glass, Acta Mater. 135 (2017) 290–296.
[61] Q. Wang, S.T. Zhang, Y. Yang, Y.D. Dong, C.T. Liu, J. Lu, Unusual fast secondary relaxation in metallic glass, Nat. Commun. 6 (2015) 7876.
[62] B. Huang, Z.G. Zhu, T.P. Ge, H.Y. Bai, B.A. Sun, Y. Yang, C.T. Liu, W.H. Wang, Hand in hand evolution of boson heat capacity anomaly and slow β-relaxation in La-based metallic glasses, Acta Mater. 110 (2016) 73–83.
[63] M.C.C. Ribeiro, Translational and reorientational heterogeneity in the glass-forming liquid $Ca_{0.4}K_{0.6}(NO_3)_{1.4}$, Phys. Chem. Chem. Phys. 6 (2004) 771–774.
[64] E.R. Weeks, D.A. Weitz, Properties of cage rearrangements observed near the colloidal glass transition, Phys. Rev. Lett. 89 (2002) 095704.
[65] B. Doliwa, A. Heuer, How do dynamic heterogeneities evolve in time? J. Non-Cryst. Solids 307-310 (2002) 32–39.